**International Journal of Mining Science (IJMS)**
*Volume 5, Issue 1, 2019, PP 11-21*
*ISSN 2454-9460 (Online)*
*DOI: http://dx.doi.org/10.20431/2454-9460.0501002*
*www.arcjournals.org*

# Formation Fragmentation Modeling and Impact on Dragline Excavation Performance in Surface Mining Operations

**Somua-Gyimah.Godfred, Frimpong.Samuel*, Nyaaba.Wedam, Gbadam.Eric**

*Department of Mining & Nuclear Engineering, Missouri University of Science & Technology, 226 McNutt Hall, 1400 N. Bishop Ave., Rolla MO 65409-0330*

***Corresponding Author:** ***Frimpong.Samuel,*** *Department of Mining & Nuclear Engineering, Missouri University of Science & Technology, 226 McNutt Hall, 1400 N. Bishop Ave., Rolla MO 65409-0330*

**Abstract:** *One aim of formation blasting is to achieve good fragmentation for excavation efficiency. When the material size distribution, which guarantees optimum dragline performance, is known, this can be used as an input for blast design. While empirical guidelines have been suggested from experimental observations, there have been no scientific studies to further explore fragmentation impact on dragline excavation efficiency. In this study, a payload model is formulated, verified and validated for simulating dragline excavation performance. The model is based on the Distinct Element Method (DEM), which simulates material flow behavior using discrete particle-to-particle interactions. An experiment was conducted to evaluate whether the payload model and the DEM technique are suitable for fragmentation studies. Generally, the results of the study confirm that the payload model can predict mean payloads, within about 17.1% mean error of experimental results. For dragline operations, the simulation results also suggest that optimum excavation efficiency is possible when formation blasting achieves a fragmentation size distribution from 0.1% to 26% of the bucket width. The dragline bucket is fully loaded (with a fill factor of 1.4) through a 5-m drag distance for 2.5 to 25 cm sized particles, whereas the bucket must be dragged through 15 m to be completely full (with a fill factor of 1.44) for 45 to 50 cm particle sizes. This study represents the first scientific investigation into the correlation between formation fragmentation and dragline excavation performance. It also presents DEM as a suitable method for formation fragmentation studies.*

**Keywords:** *Material Fragmentation, Particle Flow Code Modeling, Dragline Performance Simulation, Discrete Element Method, Numerical Simulation, Model Verification and Validation.*

## 1. INTRODUCTION

In large strip mining operations, dragline excavation is used to achieve bulk economic production targets. Strip mining operations often require pre-fragmentation of the formation prior to dragline excavation. Good fragmentation during blasting is important for excavation efficiency. When the overburden material is poorly fragmented, multiple attempts may be required to remove boulders, thereby increasing cycle time and reducing productivity. While over-fragmentation will increase the ease of excavation, it is not practical to achieve only fines through blasting. If the overburden material is over-fragmented (powdered) by blasting, the material will flow out of the rear of the dragline bucket or be blown away by gusty winds without heaping during bucket hoisting and swinging onto the spoils. This phenomenon reduces the cycle payload, and thereby reduces productivity[1]. Therefore, it is necessary to establish the optimum range of rock fragmentation sizes that have no adverse effect on excavation performance.

This is a pioneering effort to explore the fragmentation effects on dragline bucket excavation efficiency. From empirical observations, Lumley [1] concluded that for dragline excavation, good blasting should result in formation fragmentation, which consists of fines up to about 33% of the bucket width. A clearer understanding of fragmentation effects holds a lot of promise for optimizing dragline excavation efficiency. For a given excavation environment, this can be achieved by observing bucket performance for different fragmentation simulations. The optimum bucket performance output from model simulations can then be used as input for blast design to achieve the desired results.

This study pioneers an experiment to evaluate the suitability of a simulation platform, DEM, for investigating the possible excavation outcomes of different fragmentation targets during blast design.

All the studies in this report are based on the Rangal Coal Measures formation at the Newlands Mine in Australia. The results of this study are also limited to the Bucyrus Erie 1370W (BE 1370) dragline and the 47 cubic-meter ESCO Mark IV dragline bucket. The rest of this paper is organized as follows: Section 2 discusses the Distinct Element Method (DEM) and how it is used for formation excavation modeling. Section 3 introduces the forces involved in dragline excavations. Section 4 discusses the excavation simulation modeling process and Section 5 shows the model verification, validation and experimentation. Section 6 discusses the results of the experiment. Section 7 summarizes the key findings of the study.

## 2. DISTINCT ELEMENT MODELING OF DRAGLINE EXCAVATIONS

This fragmentation study was performed using the dragline excavation simulation procedure by Somua-Gyimah and Frimpong [2]. Traditionally, both soil and rock are treated as bulk material in laboratory and field tests for geomechanical design purposes. However, the objective in fragmentation studies is to analyze the material behavior due to particle interactions at the discrete level. This is not possible with finite element modeling techniques, where the material is considered as a continuum. Therefore, a discrete element approach was selected for this study to simulate the particle-to-particle interactions of fragmented, unconsolidated and granular earth material. The dragline excavation simulation model is based on the Distinct Element Method (DEM) [3]. DEM was originally developed for simulating particle-to-particle interactions of granular materials. The numerical simulation is achieved through several series of displacement and contact force calculations. These particle displacements disturb surrounding particles and govern the movement of other particles as the disturbance is propagated through the entire medium with time. DEM is based on the concept that a single time step is chosen to be very small such that particle disturbances are not propagated beyond immediate neighbors. At each time step, it is assumed that both the accelerations and velocities of all particles are constant. The movement of particles is defined by contact models, which exist at particle-particle interfaces. These particles interact at point contacts and the outcome of the interactions is determined numerically from the equations of motion using the Velocity Verlet algorithm [4]. The linear and angular accelerations ($\ddot{r}$ and $\ddot{\theta}$) of a particle, $x$, when acted upon by a moment, $M_{(x)}$ and force, $F_{(x)}$, can be derived from Newton's second law using equations (1) and (2).

$$m_{(x)}\ddot{r}_i = \sum F_{(x)_i} \tag{1}$$

$$I_{(x)}\ddot{\theta}_{(x)} = \sum M_{(x)} \tag{2}$$

$I_{(x)}$ and $m_{(x)}$ and are the moment of inertia and mass of the particle, respectively. If $\ddot{\theta}$ and $\ddot{r}$ remain constant within an infinitesimal time step, $\delta t$, the angular and linear velocities ($\dot{\theta}$ and $\dot{r}$) are also obtained from the Velocity Verlet algorithm [4] using equations (3) and (4).

$$(\dot{r}_i)_{t+\frac{\delta t}{2}} = (\dot{r}_i)_{t-\frac{\delta t}{2}} + \left(\frac{\sum\left[F_{(x)_i} + D_{(x)_i}\right]}{m_{(x)}}\right)_t \delta t \tag{3}$$

$$(\dot{\theta}_{(x)})_{t+\frac{\delta t}{2}} = (\dot{\theta}_{(x)})_{t-\frac{\delta t}{2}} + \left(\frac{\sum M_{(x)}}{I_{(x)}}\right)_t \delta t \tag{4}$$

$\sum D_{(x)}$ and $\sum M_{(x)}$ represent the sum of contact damping forces and moments respectively. Also, the angular and linear displacements ($\theta$ and $r$) of the particles are derived by integrating equations (5) and (6).

$$(r_i)_{t+\delta t} = (r_i)_t + (\dot{r}_i)_{t+\frac{\delta t}{2}} \delta t \tag{5}$$

$$(\theta_{(x)})_{t+\delta t} = (\theta_{(x)})_t + (\dot{\theta}_{(x)})_{t+\frac{\delta t}{2}} \delta t \tag{6}$$

The Newton equations (1) and (2) and finite-difference equations (3) to (6) are then repeated for each particle in the collection. Based on the material constitutive model, the force-displacement law is also used to update the forces arising from the relative motion at each contact [5]. This allows the dynamic

material behavior of the entire system to be simulated with moderate memory requirements [6]. The main limitation of DEM is the simplifying assumption that all particles only interact with one another at single contact points, rather than at multiple contact areas. The DEM formulation was implemented in the Particle Flow Code (PFC) 5.0 framework by Itasca [7].The excavation simulations were implemented in Particle Flow Code (PFC) 5.0, which is a DEM framework by Itasca [7].Figure 1 summarizes the general DEM procedure that was used in PFC 5.0 for ground excavation modeling.

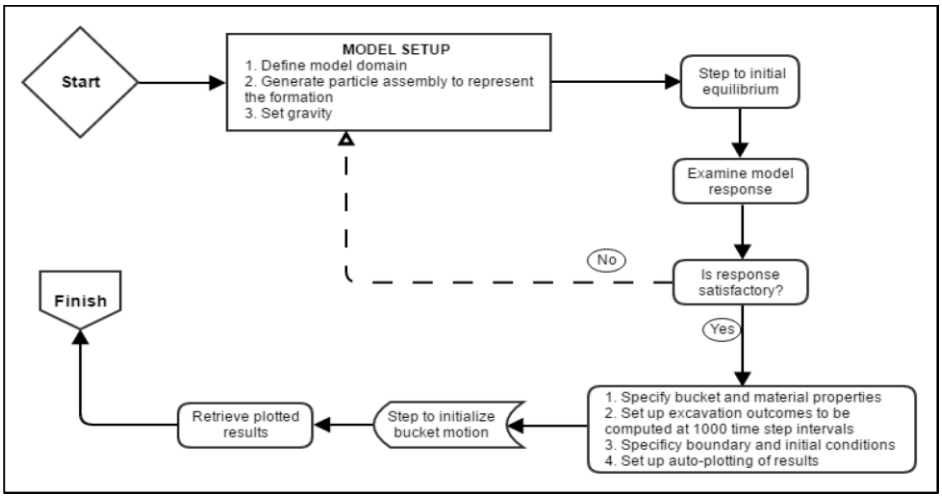


**Figure1.** *DEM procedure for excavation modeling in PFC 5.0[8]*

## 3. DRAGLINE FORCE MODELING

As shown in Figure 2, the forces acting on a dragline bucket during excavation may include the following components: (i) payload, $f_1$; (ii) frictional force generated between bucket floor and the formation, $f_2$; (iii) frictional force generated between payload and bucket floor, $f_3$; (iv) cutting force at bucket lips and teeth, $f_4$; (v) inertia force of payload, $f_5$; (vi) deadweight of the bucket, $f_6$; (vii) frictional force generated between payload and bucket sides, $f_7$; (viii) hoist force, $F_h$; (ix) drag force, $F_D$.During dragline bucket loading operations, the payload at any point in time is given by the total weight of all particles (i.e. earth material) in the bucket. For $n$ particles of mass, $m$, and occupying volume, $V$, of the bucket,the payload, $f_1$is given by equation (7).

$$f_1 = \sum_{i=1}^{n}(m_i * g) = \sum_{i=1}^{n}(\rho_f * V_i * g) = \gamma_f \sum_{i=1}^{n} V_i \quad (7)$$

$\gamma_f$ and $V_i$ are the unit weight of earth material and the volume of particle, $i$, in the bucket, respectively.

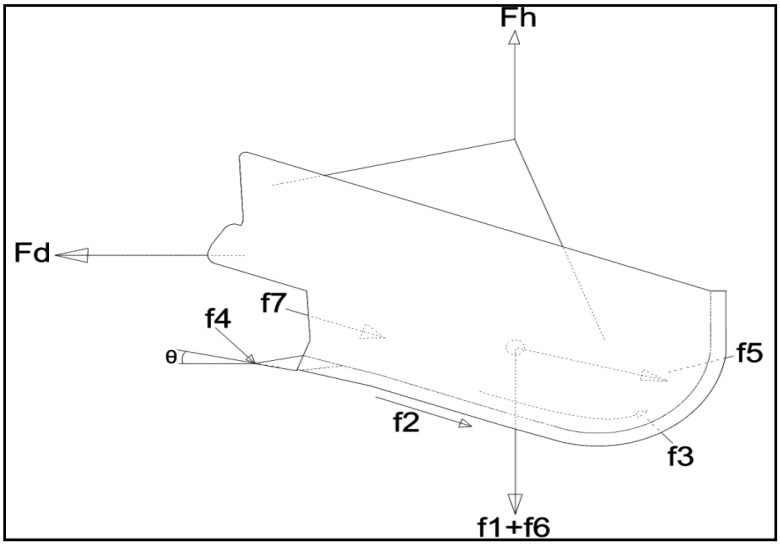


**Figure2.** *Forces on a dragline bucket during excavation*

The maximum suspended load, $M_{SL}$,is given by the sum of the bucket deadweight and the payload in equation (8).$V_b$ and $\gamma_b$ are the volume and unit weight of the bucket, respectively. The frictional forces, $f_2$ and $f_3$, are then given by equation (9) and (10), respectively.$\mu_{sm}$ is the soil-metal friction,$\alpha_f$ is introduced as a limiting factor because the value of $f_3$ is high when the bucket is near-empty but reduces with time as the material loading progresses.

$$M_{SL} = \frac{1}{g}(f_1 + f_6) = \left(\rho_f \sum_{i=1}^{n} V_i + \rho_b V_b\right) \tag{8}$$

$$f_2 = \mu_{sm}\left(\gamma_f \sum_{i=1}^{n} V_i + \gamma_b V_b\right) Cos\,\theta \tag{9}$$

$$f_3 = \mu_{sm}\left(\alpha_f \gamma_f \sum_{i=1}^{n} V_i\right);\ 0 < \alpha_f < 1 \tag{10}$$

The cutting force, $f_4$, may be expressed as the sum of all contact forces at the bucket lips and teeth. Its magnitude depends on material stiffness, bucket geometry and the drag velocity. It is assumed that the bucket dragging occurs with minimal changes in bucket velocity. The resistance forces, $f_2, f_3$ and $f_4$, are far greater than the force generated between the payload and the bucket sides, $f_7$. Therefore, $f_7$ is also assumed to be negligible. The drag force $F_D$ is given by equation (11). $\ddot{x_b}$ and $\ddot{y_b}$ are the bucket acceleration in the x- and y- directions, respectively. At any given time during the simulation, the drag energy of the bucket, $E_D$ can be determined as the sum of the kinetic energy and the work done in dragging the bucket through a horizontal distance, $x_b$ at velocity, $\dot{x_b}$[9], as given by equation (12).

$$F_D = \rho_f \ddot{x_b}\left(\sum_{i=1}^{n} V_i + \rho_b V_b\right) + \mu_{sm}\left(\gamma_f \sum_{i=1}^{n} V_i + \gamma_b V_b + \alpha_f f_1 + f_4\right) Cos\,\theta \tag{11}$$

$$E_D = \left(\rho_f \sum_{i=1}^{n} V_i + \rho_b V_b\right)\left(\frac{1}{2}\dot{x_b}^2 + g * x_b\right) \tag{12}$$

### 3.1. Dragline Payload Function

PFC 5.0 has no module for measuring excavation performance. A FISH function was therefore defined to measure the payload inside PFC 5.0 using the measurement region, as in Figure 3. The measurement region was extended beyond the struck capacity of the dragline bucket to allow for accurate measurements in case of material heaping during excavation. An extension of 50% of the bucket height was deemed sufficient because realistically, material heaping does not reach that height. After every 10,000 cycles during the simulation, the payload function loops through all the particles within the measurement region and updates the total weight using equation (1). The pseudocode for the payload-measuring FISH function is shown in Figure 4.

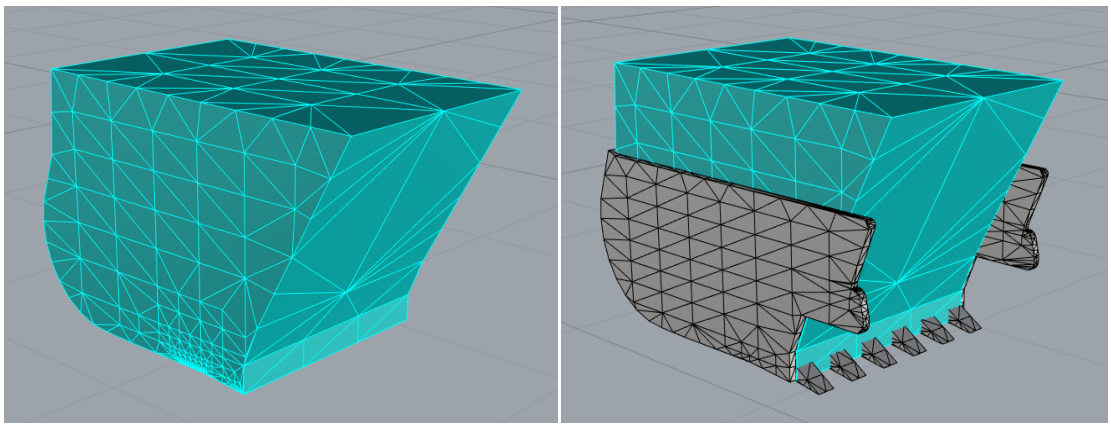

**Figure3.** *Payload-measuring region in dragline bucket [8]*

The payload measuring region is defined and initialized, as well as the mass of the material in the bucket. The particles within the measuring region are refreshed with updated masses. The coordinates of the measuring region then updated at the end of 10,000 cycles for the simulation.

***Input***: Payload measuring region, $R^p$;
***Initialize*** $R^p$;
***Define*** variable for material mass in bucket, $m_p$;
***Set*** $m_p = 0$;
***Repeat***
  ***Retrieve*** $R^p$ co-ordinates;
  ***Identify*** all balls within $R^p$ region;
  ***For each*** ball in $R^p$ region, with mass, $m_b$;
    ***Update*** $\boldsymbol{m_p}$: $m_p = m_p + m_b$
  ***Step through*** 10,000 cycles;
  ***Update*** $R^p$ co-ordinates;
***Until*** end of excavation
***Return*** $m_p$

**Figure4.** *Pseudo code for payload-measuring FISH function*

### 3.2. Bucket Payload Bulk Density Calibration

At the beginning of material simulation in PFC 5.0, the user defines a particle density for the material. PFC uses particle density, rather than bulk material density, which can be determined experimentally. For any physical material, particle density is different and often greater than the material bulk density. Since the bulk density of the virtual material is required to match that of the physical material, a fast, iterative calibration method was proposed and used in the DEM simulation. During the material generation, the initial material bulk density was determined by writing FISH functions to measure the material mass in three measurement regions, each of $1m^3$ volume. The pseudo code for the bulk density FISH function is shown in Figure 5.The measurement regions were chosen at the left, middle and right sections of the bin. The initial bulk density was then determined from the average of the densities in the three regions.

Depending on the difference between this initial bulk density and the actual bulk density of the physical material, new parameter values are then selected for the packing arrangement (material porosity) and the particle density. The two values are then varied iteratively until the bulk densities matched before running the simulation experiment. By using this approach, the bulk densities were typically matched within 3 to 5 iterations of the experiments.

## 4. EXCAVATION SIMULATION MODELING

The linear model by Cundall and Strack [6] was used as the constitutive model for the formation. The linear model (Figure 6) is based on the behavior of an infinitesimal contact surface, which permits relative rotation of the particles in contact, such as in granular materials. The contact force which governs the particle-particle interactions of the model, is given by equations (13) and (14). $F^l$ and $F^d$ are the linear elastic and dashpot force components, respectively. $\hat{n}_c$ and $\hat{t}_c$ are the unit vectors which define the contact plane.$F_n^l$ and $F_s^l$ are the respective normal and shear force components of the linear force, $F^l$. Similarly, $F_n^d$ and $F_s^d$ are the respective normal and shear force components of the dashpot force, $F^d$.

***Inputs***: Actual material bulk density, $\rho_{bulk}$, and user-defined particle density, $\rho_p$;
***Define*** three density measurement regions, $R_1, R_2$ and $R_3$, each of volume, $1m^3$.
***Define*** three mass variables, $m_1, m_2$ and $m_3$, for $R_1, R_2$ and $R_3$ respectively.
***Repeat until exit criteria is met:***
***Initialize*** material generation;
***Initialize*** $\rho_p$ and other material properties
***Cycle*** *to system stability*
***Set*** $m_1, m_2, m_3 = 0$;
***Retrieve*** $R_1, R_2$ and $R_3$ co-ordinates;
***Identify*** all balls within $R_1, R_2$ and $R_3$ regions;
***For each*** ball in $[R_1, R_2, R_3]$ with masses, $m_{b1}, m_{b2}$ and $m_{b3}$;
***Update*** $\boldsymbol{m_1, m_2, m_3}$ **such that:**

$$m_1 = m_1 + m_{b1}$$
$$m_2 = m_2 + m_{b2}$$
$$m_3 = m_3 + m_{b3}$$

***Compute model densities,*** $\rho_{m1}, \rho_{m2}, \rho_{m3}$ in $R_1, R_2$ and $R_3$ such that:

$$\rho_{m1} = m_1$$
$$\rho_{m2} = m_2$$
$$\rho_{m3} = m_3$$
$$\rho_{average} = \left(\frac{\rho_{m1} + \rho_{m2} + \rho_{m3}}{3}\right)$$

***if*** $\left|\rho_{average} - \rho_{bulk}\right| \leq (0.05 * \rho_{bulk})$, **then:**
**exit function**
***else:***
***if*** $\rho_{average} < \rho_{bulk}$, **then update** $\rho_p$ **such that:**

$$\rho_p = \rho_p + 0.1 * (\rho_{bulk} - \rho_{average})$$

***else if*** $\rho_{average} > \rho_{bulk}$, **then update** $\rho_p$ **such that:**

$$\rho_p = \rho_p - 0.1 * (\rho_{average} - \rho_{bulk})$$

**Figure5.** *Pseudo code for bulk density calibration FISH function*

$$F_c = F^l + F^d, \quad M_c \equiv 0 \tag{13}$$

$$F^l = -F_n^l \hat{n}_c + F_s^l \hat{t}_c, \qquad F^d = -F_n^d \hat{n}_c + F_s^d \hat{t}_c \tag{14}$$

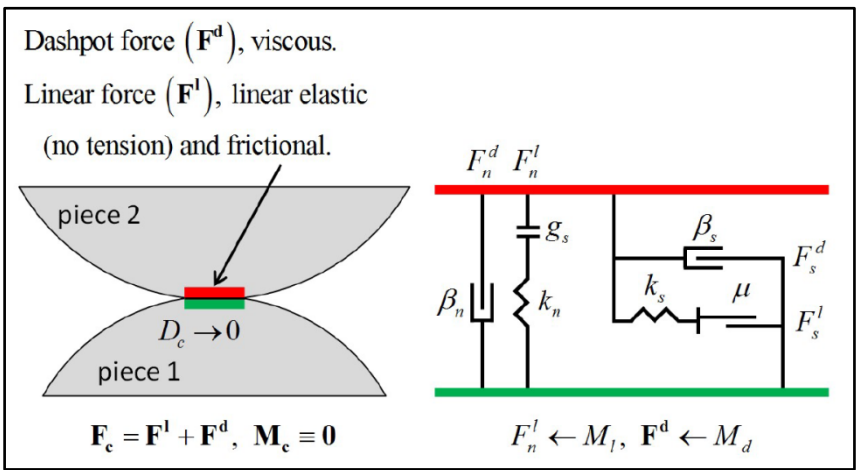


**Figure6.** *Rheological components of the linear model [7]*

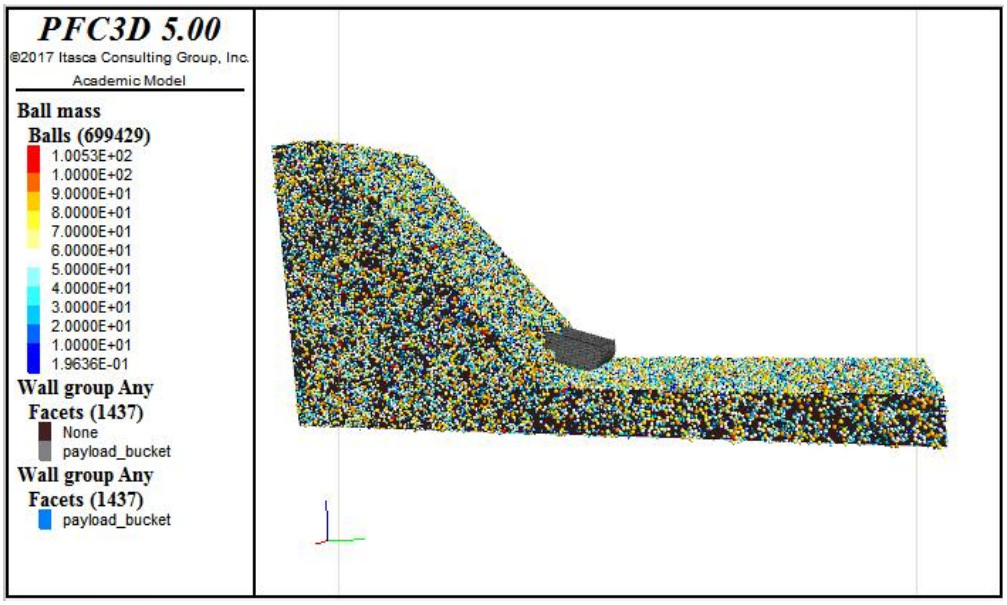


**Figure7.** *PFC Experimental model of dragline bucket loading*

The parameters of the linear model were calibrated for the formation properties using the XGBoost material calibration process by Somua-Gyimah and Frimpong [8]. The excavation simulation in PFC followed the dragline bucket-loading experiments of O'Beirne [10]. This involved the Bucyrus Erie 1370W (BE 1370) dragline and the $47m^3$ESCO Mark IV dragline bucket. Table 1 shows the characteristics of both the BE 1370 dragline and the Rangal Coal Measures overburden which were used in the study by O'Beirne [10]. Boundary conditions were generated using fixed, imaginary walls, which restrict material movement. Table 1 shows the model parameters for the simulation experiments. The full experimental setup is shown in Figure 7.

**Table1.** *Input parameters for the dragline simulation model*

| Formation Characteristics | |
|---|---|
| Formation | Rangal Coal Measures |
| Bulk Density (Kg/m3) | 1700-2300 |
| Porosity | 0.35 |
| fric | 0.87 |
| emod (GPa) | 2.82 |
| Kratio | 1.0 |
| Praticle size range (m) | 0.025-0.2 |
| Bucket – Formation friction | 0.58 |
| Damping ratio (normal) | 0.9 |
| Damping ratio (shear) | 0.9 |
| Dragline Specifications | |
| Dragline model | Bucyrus Erie 1370W (BE 1370) |
| Dragline weight | 3 500 tons |
| Boom length | 97.6 m |
| Production capacity/hour | 3 000 tons |
| Bucket model | Esco Mark IV |
| Bucket dimensions: width | 4.0 m |
| Bucket dimensions: height | 2.7 m |
| Bucket dimensions: length | 5.2 m |
| Horse power of drag motor | 1045 hp |
| Bucket weight (empty) | 37 ton |
| Bucket weight (loaded) | 73 ton |
| Rated Bucket Capacity | 42.8 $m^3$ |
| Typical bucket velocities (m/s) | 1.5-2.0 |
| Max. depth that can be worked | 38 m |
| Typical bucket velocities (m/s) | 1.5-2.0 |
| Rated Bucket Capacity | 42.8 $m^3$ |

## 5. Model Verification, Validation And Experimentation

The payload model was verified visually by comparing actual bucket loading behavior with model behavior during the simulation experiments (Figure 8). The model was observed to sufficiently simulate typical loading behaviors, such as material-pushing ahead of the bucket, as well as material heaping. The payload model was validated by comparing its digging performance with experimental results after four bucket lengths for a similar range of material densities. Table 2 shows that the mean payload from the simulation tests (95.0 tons) was only 17.1% higher than the mean payload from the actual experiments (81.1 tons). It is worth noting that the model simulates ideal conditions, where any digging constraints are fixed for all simulations. On the other hand, the experimental results represent real-life conditions, where operator inconsistencies, energy levels, operating conditions and other digging constraints make it nearly impossible for the average operator to reproduce the same excavation performance repeatedly. Also, productivity variations across the same dragline operator team have been reported to be as high as 35% [11]. Therefore, the 17.1% difference between model results and experimental results is considered acceptable. Also, a visual investigation of the results in Figure 9 shows that the model produces excavation outcomes, which fall within the ball park of experimental results.

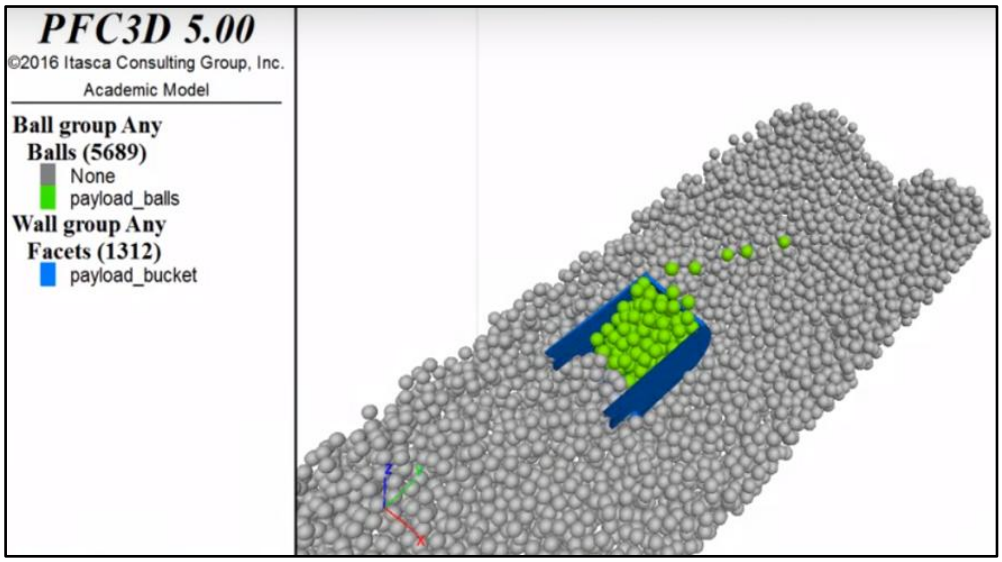


**Figure8.** *Bucket-loading process*

No previous studies have explored fragmentation effects on dragline bucket efficiency specifically. However, a clearer understanding of these effects holds a lot of promise for optimum excavation efficiency. Therefore, an experiment was carried out to better understand the effects of fragmentation on dragline excavation outcomes. In all, 5 excavation simulation tests were performed using the following material size (radius) distributions: (i) 2.5 to 25cm; (ii) 2.5 to 50cm; (iii) 20 to 25cm; (iv) 45 to 50cm; and (v) 95 to 100cm.

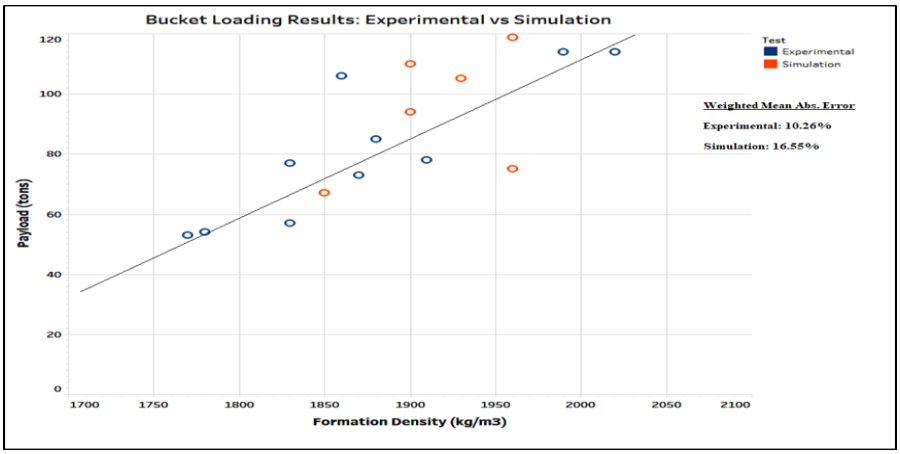


**Figure9.** *A comparison of simulation results and experimental data*

**Table2.** *Model Validation Results*

| Test | Density (kgm$^3$) | Payload (tons) | Mean Payload (tons) |
|---|---|---|---|
| Experimental | 2020 | 114 | 81.10 |
| | 1910 | 78 | |
| | 1780 | 54 | |
| | 1860 | 106 | |
| | 1830 | 77 | |
| | 1770 | 53 | |
| | 1990 | 114 | |
| | 1880 | 85 | |
| | 1830 | 57 | |
| | 1870 | 73 | |
| Simulation | 1960 | 119 | 95.00 |
| | 1960 | 75 | |
| | 1900 | 94 | |
| | 1900 | 110 | |
| | 1850 | 67 | |
| | 1930 | 105 | |

## 6. Results And Discussion Of Experimental Results

Material size distribution and drag time can be used to optimize dragline performance in any formation. Figures 10 shows the results of material size distribution in dragline performance for 15 meters of dragging. Generally, the loading profiles of various material size distributions follow expected trends. After about half a bucket length of dragging (2.5m), the formation with the smallest material size range (2.5 to 25cm) recorded the highest payload (42 tons), whilst the formation with the largest size distribution (95 to 100cm) recorded the lowest payload (5 tons). Similarly, the initial payload for the other three tests decreased as the material size distributions increased(2.5 to 25 cm, 2.5 to 50 cm, 20 to 25cm, 45 to 50cm and 95 to 100 cm). The bucket is completely filled after 5-m drag distance with the finest materials (2.5 – 25 cm size distribution) and after 7.5-m dragging with the material of 2.5 – 50 cm size distribution. The bucket is completely filled after 10-m dragging with 20 – 25 cm and 45 – 50 cm material size distributions. Finally, the bucket is completely filled after 15-m dragging with 95 – 100 cmsize distribution.

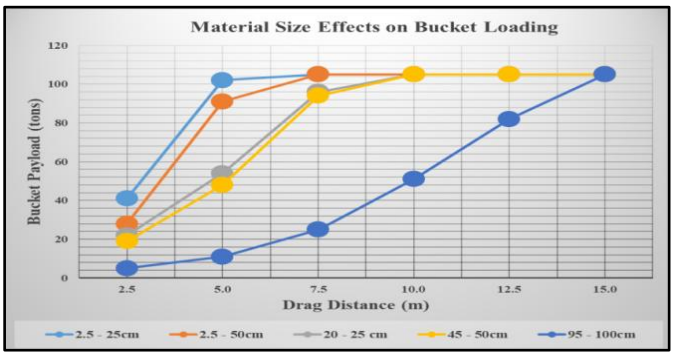


**Figure10.** *Effects of material size (radius) on bucket loading.*

For granular earth materials, this observation corresponds to normal behavior. This is because finer discrete particles will generally offer less resistance to excavation, as compared to larger, blocky particles. The same trend was observed at one bucket length (5m). However, after a drag distance of 1.5 times the bucket length (7.5m), the formation with the largest size distribution only achieves a 34% bucket fill factor (24 tons). By contrast, the other four formations exceed 100% fill factor within the same drag distance (Figure 11). The bucket achieves 1.4 fill factor after 5-m drag distance within the finest materials (2.5 – 25 cm size distribution) and 1.44 fill factor after 7.5-m dragging with the material of 2.5 – 50 cm size distribution. The bucket also achieves 1.44 fill factor after 10-m dragging within 20 – 25 cm and 45 – 50 cm material size distributions and after 15-m dragging with 95 – 100 cm size distribution. Overall, the observations in this experiment support the theory that bucket loading behavior is strongly influenced by the material size distribution of the formation. Generally, the smaller the material size distribution, the better the loading performance.

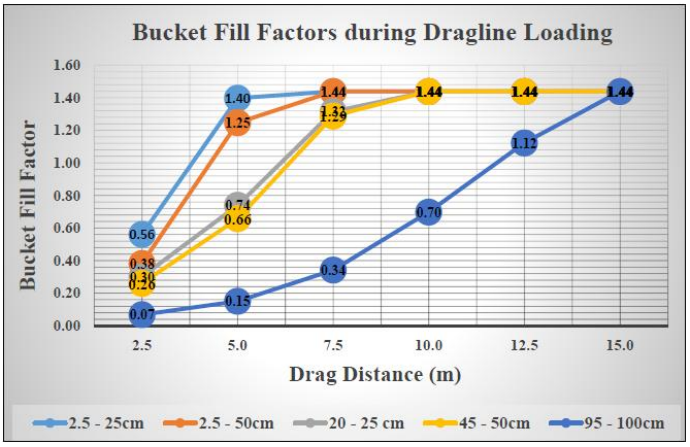


**Figure11.** *Bucket Fill Factors during Dragline Loading*

For a bucket width of 3.9m, the formations with material sizes within 26% of the bucket width (50cm radius) were able to reach full bucket capacity (i.e. fill factor ≥ 1.0) in relatively the same amount of time. On the other hand, the formation with material sizes greater than 26% required considerably more time to reach full bucket capacity (Figures 10 and 11). Lumley [1] suggested that blast design for efficient dragline excavation should target a material size distribution from fines up to a third of the bucket width. The observations in this study generally support the assertions by Lumley [1] and show that optimum excavation performance could be obtained when the formation fragments range from fines up to about a quarter of the bucket width as illustrated in Figures 10 and 11.

## 7. CONCLUSION

Good fragmentation during blasting is important for excavation efficiency. When the material size distribution for optimum dragline performance is known, it can be used as an input for blast design. While empirical guidelines have been suggested by Lumley [1]. There have been no scientific studies to further explore fragmentation effects on dragline excavation efficiency. A DEM model was formulated, verified and validated for predicting dragline bucket payload. The model achieves slightly different (17.1% higher) excavation results from actual experiments. However, this difference is considered acceptable since productivity variations across the same dragline operator team have been reported to be as high as 35% [11]. An experiment was conducted to evaluate whether the DEM technique can be successfully used for fragmentation studies. The results show that optimum excavation efficiency is possible when formation blasting achieves a fragmentation size distribution within a range of 0.1% to 26% of the bucket width. These results largely agree with the earlier results from Lumley [1], who suggested an optimum range of fines to 33% from his observations. This suggests that the DEM-based payload model can obtain excavation results that are backed by both empirical evidence and experimental studies, within a reasonable margin of error. This study represents the first scientific investigation into the correlation between formation fragmentation and dragline excavation performance. It also presents DEM as a suitable method for formation fragmentation studies.

## REFERENCES

[1] Lumley, G., Dragline Dictionary: PwC – Mining Intelligence and Benchmarking, P. Coopers, Editor. 2014.

[2] Somua-Gyimah, G., et al., A Material Flow Model for Dragline Bucket-Formation Failure Analyses Using the Distinct Element Method. International Journal of Mining Engineering and Technology, 2018. 1(1): p. 1-15.

[3] Cundall, P. A computer model for simulating progressive large-scale movements in block rock mechanics. in Proc. Symp. Int. Soc. Rock Mech. Nancy. 1971.

[4] Verlet, L., Computer" experiments" on classical fluids. I. Thermodynamical properties of Lennard-Jones molecules. Physical review, 1967. 159(1): p. 98.

[5] Lim, W.L., Mechanics of railway ballast behaviour. 2004, University of Nottingham.

[6] Cundall, P.A. and O.D. Strack, A discrete numerical model for granular assemblies. Geotechnique, 1979. 29(1): p. 47-65.

[7] Itasca, PFC 5.0 Documentation. 2013.

[8] Somua-Gyimah, G., et al., A machine learning approach to DEM material model calibration. 2018.

[9] Leonides, C., Control and Dynamic Systems V34: Advances in Control Mechanics Part 1 of 2: Advances in Theory and Applications. 2012: Academic Press.

[10] O'Beirne, T.J., Investigation Into Dragline Bucket Filling: Final Report : ACARP Project C3002. 1997: Australian Coal Association Research Program, Australian Coal Industry Research Laboratories.

[11] Lumley, G., Reducing the variability in dragline operator performance. 2005.

**Citation:** *Frimpong.Samuel, et.al. (2019)" Formation Fragmentation Modeling and Impact on Dragline Excavation Performance in Surface Mining Operations", International Journal of Mining Science (IJMS), 5(1), pp.11-21, DOI: http://dx.doi.org/10.20431/2454-9460.0501002*